Assessment of Wall Modeling With Adverse Pressure Gradient for High Reynolds Number Separated Flows

Sajad Mozaffari, Jérôme Jacob, Pierre Sagaut

Assessment of wall modeling with adverse pressure gradient for high Reynolds number separated flows

Sajad Mozaffari[1*], Jérôme Jacob[1] and Pierre Sagaut[1]

[1]M2P2 UMR 7340, Aix Marseille Univ, CNRS, Centrale Marseille, Marseille, 13451, France.

*Corresponding author(s). E-mail(s): sajad.mozaffari@univ-amu.fr;
Contributing authors: jerome.jacob@univ-amu.fr; pierre.sagaut@univ-amu.fr;

Abstract

This paper applies a recently developed approach for modeling turbulence near wall regions within a lattice Boltzmann solver, in combination with a Hybrid RANS/LES turbulence model, to study turbulent separated flows at high Reynolds numbers. To simulate unsteady detached flows on a non-body-fitted Cartesian grid, wall models are employed to estimate the effects of unresolved near-wall turbulence on the overall flow. The article presents the extension of an equilibrium power law wall model to handle adverse pressure gradients (APGPL) and its application in simulating external aerodynamic flows. Hybrid RANS/LES simulations are conducted for two challenging test cases: a 3D NACA-4412 airfoil near stall and a complex Ahmed body configuration. Comparison with a reference simulation involving resolved boundary layers and experimental data demonstrates the strong performance of the wall model, when considering adverse pressure gradients, in simulating turbulent boundary layers under various conditions, ranging from fully attached to mild to high adverse pressure gradients.

Keywords: Hybrid RANS/LES, Lattice Boltzmann Method (LBM), Wall modeling, High Reynolds number, Separated flow

1 Introduction

Wall modeling holds paramount significance in the field of computational fluid dynamics (CFD), particularly for simulating turbulent flows with high Reynolds numbers in the vicinity of solid surfaces. In the context of the lattice Boltzmann method (LBM), due to the isotropic

behavior of structured mesh generation methods, refining grids to resolve near-wall turbulence would result in an excessively high computational cost. Therefore, it is necessary to use wall models to represent the effects of the unresolved near-wall region on the outer layer.

Numerous wall models have been developed to address the issue of predicting the velocity profile within the near-wall region. The most commonly used wall model relies on a wall law of the velocity and a simple algebraic relationship to evaluate wall shear stress at the first off-wall grid point. For instance, In the absence of pressure gradient effects on the boundary layer, the velocity profile can be assumed to satisfy a logarithmic law [1, 2]:

$$u(y) = u_\tau \left[\frac{1}{\kappa} \log\left(\frac{y u_\tau}{\nu} \right) + B \right], \tag{1}$$

where κ denotes the von Kármán constant and B is an intercept coefficient. These models are implicit, and an iterative method is needed for solving the nonlinear equation for the wall friction velocity, u_τ. This iterative method is time-consuming and may introduce numerical errors in the determination of flow quantities at the boundary nodes.

Other algebraic closures of the wall stress are also available that rely on different assumptions on the shape of the velocity profile, potentially accounting for the viscous sublayer and buffer layer [3–5]:

$$u(y) = u_\tau C_{pow} \left(\frac{y u_\tau}{\nu} \right)^\alpha, \tag{2}$$

where the coefficient C_{pow} and the power α are generally assumed Reynolds number dependent. This explicit power law model provides an alternative to the log law, where an explicit expression of the wall shear stress is proposed in terms of the velocity vector at the first grid point. Wilhelm et al. [6], in the LBM framework, proposed an explicit wall model based on the power law wall model in conjugation with the immersed body (IB) boundary condition for the non-body fitted meshes. This model does not rely on an iterative procedure for the determination of the friction velocity. Moreover, its use on Cartesian grids is very simple and enables the evaluation of the velocity at boundary nodes without the previous determination of the friction velocity. Cai et al. [7] also developed an explicit model allowing straightforward evaluation of the friction velocity on near-wall grids independent of their locations in the turbulent boundary layer.

The theoretical basis of these wall models is the universal behavior of attached boundary layers described by the law of the wall, which is based on the wall shear stress. Therefore, separation and reattachment are the two standard flow situations in which the law of the wall based on the wall shear stress fails. This can impose non-physical perturbations in the case of a boundary layer under an adverse pressure gradient and in particular for separated boundary layers [8]. This problem has been addressed by several studies taking the streamwise pressure gradient into account based on log law models [9–11], and power law models [12–14], assuming that the pressure is constant in the wall-normal direction and the pressure gradient acts mainly in the streamwise direction [15]. Among these attempts, the proposed model by Afzal et al. [9], by imposing the effect of adverse pressure gradient into their log law wall model, gave a better representation of the velocity profile in a boundary layer under adverse pressure gradient than the classical log law. The Afzal wall law has been successfully used for the prediction of various flows under adverse pressure gradients involving separation (e.g. a single cylinder [16], tandem cylinders [17], and airfoil [18, 19]).

Regardless of the success of these models in their field of development, they can not extend their application in all internal and external turbulent separated flows. These wall models are still not valid at a separation or reattachment point where friction velocity u_τ becomes zero. Recently, Wilhelm et al. [20] extended the equilibrium power law wall model to an adverse pressure gradient power law (APGPL) for boundary layers under an adverse pressure gradient in order to mimic an implicit non-equilibrium log law based on the Afzal model [9]. The model behaves as the equilibrium power law in regions of no or favorable pressure gradient. In regions of adverse pressure gradient, the APGPL mode of the wall model is activated, and in separated flow regions, the no-slip boundary condition using linear/quadratic interpolation for the determination of the velocity on the first off-wall nodes is applied. This shows success in several WMLES simulations of external aerodynamics flow under high adverse pressure gradient and fully attached flows e.g. airfoil in a stall situation.

In this study, the potential of the APGPL model in conjunction with the IDDES hybrid RANS/LES turbulence model in the LBM framework is investigated. In boundary layers subjected to adverse pressure gradients, equilibrium wall models fail to exhibit consistent behavior and are unable to accurately capture local flow structures, such as minor separation and its subsequent reattachment (as reported by Mozaffari et al. [8] for IDDES simulations and Menter et al. [21] for WMLES simulations of the turbulent separated flow over Ahmed's body configuration). The primary objective of this research is to investigate the significant effect of incorporating adverse pressure gradients into the wall model for more effective and reliable simulations in the realm of turbulent separated flows. This extends the application of the wall model within the LBM framework to complex and challenging aerodynamic external flows, with a particular focus on capturing local flow structures. The paper proceeds by introducing the numerical methods employed in Section 2. The ProLB solver is introduced, along with a brief description of the lattice Boltzmann method and the IDDES (Improved Delayed Detached Eddy Simulation) turbulence model which was implemented based on the k-ω SST RANS model within the ProLB solver and validated for turbulent flows at high Reynolds number. Furthermore, a concise description of the APGPL power law wall model is presented in the same section. To demonstrate the model's performance in predicting wall components for turbulent boundary layers under varying adverse pressure gradients, two challenging turbulent flows are considered in Section 3: a 3D NACA-4412 airfoil operating close to the stall position, where trailing edge separation occurs, and a complex and realistic test case involving an Ahmed body. In both cases, the prediction of a separated boundary layer on the body's surface proves to be particularly challenging. For each test, comparisons are made with reference simulations and experimental data, and the impacts of the wall model are thoroughly discussed. Finally, the study offers conclusions in Section 4.

2 Numerical methods

This study is based on a research version of the commercial LBM solver, ProLB [22], developed as part of a scientific collaboration involving CSSI, Renault, Airbus, Safran, École Centrale de Lyon, CNRS, and Aix-Marseille University. In this section, the Lattice Boltzmann method is briefly explained, along with an introduction to the IDDES hybrid RANS/LES turbulence model used for simulating unsteady turbulent flows. Furthermore, the text describes the near-wall treatment implemented in the ProLB solver to prevent excessively

refined Cartesian grids near solid boundaries, particularly in high Reynolds number flows. An overview of the Adverse Pressure Gradient power law (APGPL) wall model, as introduced by Wilhelm et al. [20], is also provided to address boundary layers under adverse pressure gradients.

2.1 Lattice Boltzmann method and Turbulence Modeling

2.1.1 Lattice Boltzmann Method (LBM)

The LBM is based on the statistical mechanics of particles at a mesoscopic scale. This approach describes the dynamics of a group of particles that collide and propagate over a discrete lattice based on the discrete velocity Boltzmann equation:

$$\frac{\partial f_i}{\partial t} + \mathbf{c}_i \cdot \nabla f_i = \Omega_i. \tag{3}$$

The fundamental quantity in this method is the probability distribution function $f_i(t, \mathbf{x}, \mathbf{c}_i)$, which characterizes the probability of encountering a particle with a discrete velocity $\mathbf{c}_i$ at the position $\mathbf{x}$ and time t. In the ProLB solver, the Boltzmann equation is discretized within a 3D lattice, employing 19 discrete velocities (D3Q19). By employing the trapezoidal rule to discretize the discrete velocity Boltzmann equation, following a change of variables $\bar{f}_i = f_i - \Delta t \Omega_i/2$, an explicit scheme is obtained, as detailed in [23]:

$$\bar{f}_i(t + \Delta t, \mathbf{x} + \mathbf{c}_i \Delta t) - \bar{f}_i(t, \mathbf{x}) = \Delta t \cdot \bar{\Omega}_i(t, \mathbf{x}), \tag{4}$$

where the collision operator $\bar{\Omega}_i(t, \mathbf{x})$, models particle interactions as they relax towards an equilibrium state f_i^{eq} :

$$\bar{\Omega}_i(t, \mathbf{x}) = -\frac{1}{\bar{\tau}}(\bar{f}_i - f_i^{eq}), \tag{5}$$

where the relaxation time $\bar{\tau} = \tau + 0.5$ is related to the fluid kinematic viscosity ($\tau = \nu/c_s^2$). The Maxwell–Boltzmann equilibrium expanded in Hermite polynomials is given by

$$f_i^{eq} = w_i \rho \left(1 + \frac{\mathbf{u} \cdot \mathbf{c}_i}{c_s^2} + \frac{1}{2c_s^4} \mathbf{H}_i^{(2)} : \mathbf{uu}\right). \tag{6}$$

In Eq. 6, ρ and $\mathbf{u}$ represent the fluid density and velocity, respectively, which are reconstructed using probability distribution functions as follows:

$$\rho(t, \mathbf{x}) = \sum_i \bar{f}_i(t, \mathbf{x}), \tag{7}$$

$$\rho \mathbf{u}(t, \mathbf{x}) = \sum_i \mathbf{c}_i \bar{f}_i(t, \mathbf{x}). \tag{8}$$

Additionally, w_i is the weighting factor dependent on the discrete velocity direction, and the second-order Hermite polynomial ($\mathbf{H}_i^{(2)}$), with the identity matrix $\mathbf{I}$, is defined as:

$$\mathbf{H}_i^{(2)} = \mathbf{c}_i \mathbf{c}_i - c_s^2 \mathbf{I}. \tag{9}$$

Due to the instability of the original collision operator in most practical applications at high Reynolds number flows, a hybrid recursive regularized (HRR) collision operator [24] is developed. This operator decomposes the distribution function into an equilibrium and a non-equilibrium part ($\bar{f}_i = f_i^{eq} + f_i^{neq}$), expands the non-equilibrium part of the particle distribution function (f_i^{neq}) into a Hermite series, and introduces hyperviscosity as follows:

$$\bar{\Omega}_i^{HRR}(t,\mathbf{x}) = -\frac{1}{\bar{\tau}}\left(f_i^{neq}\sigma - (1-\sigma)\frac{\rho\bar{\tau}}{c_s^2}\mathbf{H}_i^{(2)} : \mathbf{S}^{\mathrm{FD}}\right). \tag{10}$$

Here, $\mathbf{S}^{\mathrm{FD}}$ represents the strain rate tensor, which is evaluated using finite difference. The level of hyperviscosity for stabilization is controlled by the value of σ, which is selected to be as close to unity as possible (for more information, please refer to [24]). Turbulence effects are incorporated into the collision operator through the relaxation time $\bar{\tau}$ towards equilibrium. The eddy viscosity ν_t, calculated by turbulence models, is introduced into the relaxation time of the regularized collision model as:

$$\bar{\tau} = \frac{\Delta t}{2} + \frac{\nu + \nu_t}{c_s^2}, \tag{11}$$

where c_s is the lattice speed of sound. For a comprehensive introduction to the fundamental theory of the Lattice Boltzmann Method (LBM) and its applications, please refer to the book by Krüger et al. [25].

2.1.2 Turbulence model

The ProLB solver was initially developed for performing wall-modeled LES (WMLES) simulations in non-body-fitted computational domains. This solver also validated a Spalart-Almaras (SA) RANS turbulence model for external aerodynamics applications[6, 26, 27], and it has been widely adopted. While modeling local flow features like attached boundary layers is more effective using a RANS model, simulating complex, unsteady flows at high Reynolds numbers poses challenges. Local flow separations and the necessity for accurately resolving unsteady features make LES a more suitable choice. However, performing LES to resolve near-wall turbulence remains computationally demanding due to the need for locally fine grids near the walls. Therefore, the hybrid RANS/LES approach, which involves using LES in the separated flow region to capture three-dimensional, time-dependent flow features and a RANS model in the attached boundary layers near the wall to avoid the need for excessively fine grids, has attracted significant interest within the framework of LBM.

In the ProLB solver, due to the robustness of the two-equation RANS model, particularly the k-ω SST model, for attached flows, it was selected as a basis for the hybrid RANS/LES turbulence model. Among several hybrid RANS/LES turbulence models, IDDES shows promising results for simulating highly unsteady flows, including separation [28]. The principle of this model is to perform RANS within the boundary layer and near the wall, and LES simulations in the far-field regions. IDDES, being a more recent iteration of the original DES model [29] which is based on a modification of the Spalart-Allmaras one-equation model [30]. The primary limitation of the DES model was related to a specific transition region downstream of the RANS-LES interface, which was referred to as the *grey area*. At the

RANS-to-LES interface, the modeling is switched instantly from a non-turbulence-resolving method to a turbulence-resolving method across a single grid plane. The eddy viscosity is reduced, and therefore the modeled Reynolds stress drops. However, the resolved turbulent stresses associated with the resolved flow unsteadiness are not instantly fully developed to replace this reduction of the modeled turbulence. Since in the incoming RANS-simulated flow, there are no or only weak natural instabilities, a certain transition region downstream of the RANS-LES interface is needed for the LES-simulated flow to develop resolved turbulence - if it develops at all. The effect of this transition region was detected among the first test cases [31] in which the DES model was used and is referred to as modeled-stress depletion (MSD). The impact of the grey area becomes significantly more pronounced when transitioning from RANS to LES mode within the attached boundary layer. In severe cases, this transition can result in grid-induced separation (GIS) [32].

Consequently, the IDDES model [33, 34], similar to its predecessor, Delayed Detached Eddy Simulation (DDES) [35], serves as a shield against grid-induced separation, preventing an abrupt shift to LES mode within the boundary layer. Additionally, it allows the model to operate in Wall-Modeled LES (WMLES) mode when simulating wall boundary layers under unsteady inlet conditions. This approach provides a flexible and convenient scale-resolving simulation (SRS) model suitable for high Reynolds number flows. The underlying principle of this hybridization method was extended to the two-equation k-ω SST turbulence model [36] through a careful adjustment of the reference length scale. This adjustment is aimed at modifying the dissipation term in the k-equation of the SST model [33]:

$$\frac{\partial k}{\partial t}+\frac{\partial (u_j k)}{\partial x_j}=\tau_{ij}\frac{\partial u_j}{\partial x_j}-\beta^*\omega k+\frac{\partial}{\partial x_j}\left[(\nu+\sigma_k\nu_t)\frac{\partial k}{\partial x_j}\right], \tag{12}$$

$$\beta^*\omega k \rightarrow \beta^*\omega k F_{IDDES}, \tag{13}$$

$$F_{IDDES}=\frac{l_{RANS}}{l_{IDDES}}, \tag{14}$$

where

$$l_{IDDES}=\hat{f}_d\cdot(1+f_e)\cdot l_{RANS}+(1-\hat{f}_d)\cdot l_{LES}. \tag{15}$$

The $\hat{f}_d$ is an empirical blending function that combines the two branches DDES and WMLES. The elevating function f_e is also defined to prevent the excessive reduction of the RANS Reynolds stresses in the vicinity of the RANS and LES interface and to ensure that the log-layer mismatch does not occur. A detailed description of these functions can be found in [33].

Further discussions on this hybridization method based on the k-ω SST turbulence model within the LBM can be found in the work by Mozaffari et al. [8].

2.2 Near-wall treatment

In ProLB, the LBM is applied on a Cartesian grid which is not body-fitted, as illustrated in Figure 1. The *boundary nodes* do not necessarily lie on the solid boundary and the LBM scheme is not completed at these off-surface nodes (boundary nodes). Therefore, a reconstruction method should be used to estimate the velocity at the boundary nodes from the velocity predicted at neighboring fluid nodes.

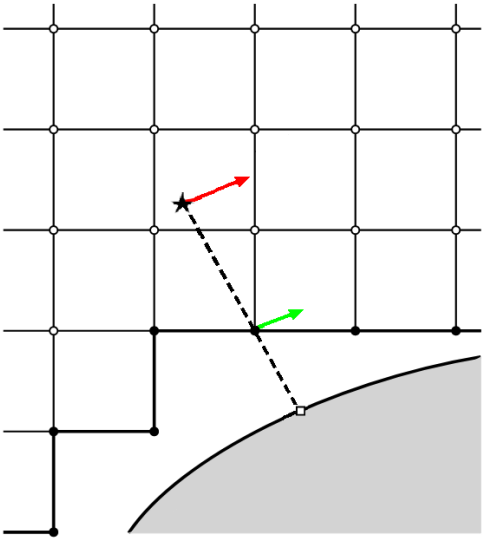

Fig. 1: Cartesian grid in LBM and wall treatment strategy to apply the tangential velocity boundary condition; ●: boundary node, ○: fluid node, ⋆: reference point, and □: projected surface points.

In ProLB, based on the immersed boundary (IBM) approach, several fictitious reference points are established along the wall-normal direction passing the boundary points at a distance of the local grid size successively, which their values are interpolated from the neighbor points [26]. Then, the flow quantities (e.g. velocity or density) at boundary nodes are constructed, linearly or quadratically, based on the boundary type, Dirichlet boundary condition (e.g. inflow velocity, or no-slip velocity), or Neumann boundary condition (e.g. outflow velocity). Thanks to the regularized approach, the macroscopic boundary conditions can be easily transformed into the particle distribution functions for LBM. The equilibrium part is reconstructed from the flow velocity and density, while the non-equilibrium part can be computed from the symmetric part of the velocity gradient tensor. To obtain accurate results, advanced gradient schemes have been used on the boundary nodes, cf. [26, 27, 37].

Additionally, for high Reynolds number flows, due to the mesh isotropy in ProLB, it is too expensive to sufficiently refine the grids in the wall-normal direction near a solid boundary in order to explicitly resolve the boundary layer. Therefore, a wall model, based on the tangential velocity at these reference points, can determine the tangential velocity and the quantities related to the turbulence model of the first off-wall node. According to this, the velocity direction matches the tangential velocity at the reference point (Figure 1, see [6]).

In ProLB, various wall models are available to describe the velocity profile in the turbulent boundary layer by establishing a relationship between tangential velocity, distance from the wall, and friction velocity. Wilhelm et al. [6] introduced an algebraic wall model, rooted in a power law velocity profile. Notably, this model eliminates the need for an iterative process, which is common in conventional methods, to determine the wall shear stress. Similarly, Cai et al. [7] developed a fully explicit algebraic wall model that encompasses the

entire inner region of the turbulent boundary layer, reducing computational requirements for wall-bounded turbulent flows. Both of these wall models assume the boundary layer is in equilibrium. However, Mozaffari et al. [8] demonstrated that applying an equilibrium wall model can introduce non-physical perturbations, particularly in cases of boundary layers under adverse pressure gradients and separated boundary layers.

More recently, Wilhelm et al. [20] expanded the equilibrium power law wall model to address boundary layers subject to adverse pressure gradients. They developed a novel explicit wall model based on an existing log law for adverse pressure gradients [9]. This new model, known as the Adverse Pressure Gradient power law (APGPL) model, comprises three modes that can be simultaneously active in various regions of a flow. In regions of favorable or no pressure gradient, where the streamwise pressure gradient $dp/ds(\mathbf{x},t) \leq 0$, the equilibrium power law is used:

$$u^+ = \begin{cases} y^+ & \text{if } y^+ \leq y_c^+ \\ A\left(y^+\right)^B & \text{if } y^+ \geq y_c^+ \end{cases} \tag{16}$$

where $B = 1/7$ and $y_c^+ = 11.81$ is the scaled height of the viscous sub-layer. By continuity of the velocity profile at $y_c^+, A \approx 8.3$. The scaling is based on the friction velocity u_τ such as:

$$u^+ = \frac{u}{u_\tau} \quad \text{and} \quad y^+ = \frac{y u_\tau}{\nu} \tag{17}$$

In this work, the explicit expression of the equilibrium power law model as defined by Wilhelm et al. [6] for u_τ:

$$u_\tau = \begin{cases} \sqrt{\frac{\nu u}{y}} & \text{if } y^+ \leq y_c^+ \\ u^{\frac{1}{1+B}} A^{\frac{-1}{1+B}} y^{\frac{-B}{1+B}} V^{\frac{B}{1+B}} & \text{if } y^+ \geq y_c^+ \end{cases} \tag{18}$$

In regions exposed to adverse pressure gradients, the APGPL is used.

$$u^+ = \begin{cases} y^+ & \text{if } y^+ \leq y_c^+ \\ A\left(y^+\right)^B + \alpha\sqrt{y^+ p^+} + \beta\left(p^+\right)^{1/3} \ln\left(\gamma\left(y^+\right)^3 p^+\right) & \text{if } y^+ > y_c^+ \end{cases} \tag{19}$$

where $B = 1/7$, $A \approx 8.3$, $\alpha = 7.5789$, $\beta = -1.4489$, $\gamma = 191.1799$. For $y^+ > y_c^+$, the explicit expression of the APGPL model for u_τ can be written as:

$$u_\tau = A^{\frac{-1}{B+1}} \left(\frac{\nu}{y}\right)^{\frac{B}{B+1}} \left(u - \alpha\sqrt{\frac{y}{\rho}\frac{dp}{ds}} - \beta\left(\frac{\nu}{\rho}\frac{dp}{ds}\right)^{1/3} \ln\left(\gamma\frac{y^3}{\rho\nu^2}\frac{dp}{ds}\right)\right)^{\frac{1}{B+1}}. \tag{20}$$

In real-flow applications featuring diverse flow regions, the areas experiencing adverse pressure gradients can be identified by $dp/ds(\mathbf{x},t) > 0$ and $D(\mathbf{x},t) \geq 0$, where D is defined as follows:

$$D = u - \alpha\sqrt{\frac{y}{\rho}\frac{dp}{ds}} - \beta\left(\frac{\nu}{\rho}\frac{dp}{ds}\right)^{1/3} \ln\left(\gamma\frac{y^3}{\rho\nu^2}\frac{dp}{ds}\right) = A\left(u_\tau\right)^{B+1}\left(\frac{y}{\nu}\right)^B. \tag{21}$$

At a separation or reattachment point, where the friction velocity u_τ becomes zero, the wall model is deactivated, and the boundary layer is resolved with a no-slip boundary condition. In this scenario ($dp/ds(\mathbf{x},t) > 0$ and $D(\mathbf{x},t) < 0$), the wall shear stress $\tau_w = \rho u_\tau^2$ is computed based on the assumption of a linear velocity profile near the wall. Linear behavior is well known to hold for the case of the smooth wall viscous sublayer [38]. Therefore, the friction velocity is given by:

$$u_\tau = \sqrt{\frac{\nu \|u\|}{y}}, \tag{22}$$

where $\|u\|$ represents the norm of the tangential velocity derived from the no-slip boundary condition. Additional detailed information regarding the APGPL wall model can be found in [20].

The objective of this study, owing to the initial promising outcomes of the APGPL model, is to explore the potential of the APGPL model when used alongside the IDDES hybrid RANS/LES turbulence model. This combined approach is applied to address two particularly challenging scenarios, with a specific focus on the accurate representation of local flow structures and the prediction of separation. Notably, in these scenarios, prior attempts to employ an equilibrium wall model in conjunction with a hybrid RANS/LES turbulence model within the LBM framework have failed to accurately capture the complexities of separated boundary layers. This research serves as an important step in the quest for more effective and reliable simulation techniques in the context of turbulent separated flows.

3 Results and discussion

This section outlines the simulation setup for a 3D airfoil and Ahmed's body, along with the presentation of results and their analysis. A 3D NACA 4412 airfoil near stall is selected to assess the performance of the APGPL model in conjunction with the IDDES hybrid turbulence model. This evaluation aims to predict the flow in fully turbulent attached and separated boundaries, showcasing the model's capability in accurately predicting the small separation at the trailing edge. Additionally, an Ahmed body with two slant angles is considered to illustrate improvements in representing flow structures on the slant and in the wake of the body. This improvement is attributed to the application of a wall model that takes into account the adverse pressure gradient, in contrast to the solution reported by Mozaffari et al. [8], employing an equilibrium wall model.

3.1 3D NACA 4412 airfoil

The first test case is a NACA 4412 airfoil with a chord (c) of 0.7454 m and a span (s) of $20\%c$. For this study, according to the experimental study of Wadcock (1987) [39], the airfoil is exposed to a turbulent flow with $Ma = 0.085$ which is associated with a chord-based Reynolds number $Re_c = 1.64 \times 10^6$ at maximum lift configuration (angle of attack $\alpha = 12^\circ$). The objective is to assess the performance of the APGPL wall model in predicting the trailing edge separation.

The computational domain is chosen in a way that the distance between the inlet and the airfoil is 30 times of the chord length ($x/c = -30$) and the outlet is located at $x/c = 60$ behind the airfoil. Also in the Y direction, the top and bottom boundaries are at $y/c = \pm 30$.

Regarding the boundary conditions, the free-stream velocity is imposed at the inlet and the bottom boundaries with an angle corresponding to the angle of attack. For the outlet and top boundaries, the constant density condition is applied. A periodic boundary condition is adopted in the spanwise direction. Moreover, a fixed velocity and a fixed density sponge layers [40] are also defined at the inlet and outlet boundaries, respectively, to ensure convergence toward a steady state and prevent spurious reflection of disturbances.

Table 1: Mesh resolution used within this study.

Mesh name	$L \times H \times W$ ($\times C^3$)	Δx_{max}	Δx_{min}	N° of cells	$y^+(\approx)$
Medium (M)	$91 \times 61 \times 0.2$	0.0745 (10%C)	0.001164 (0.15%C)	12.5M	250
Fine (F)	$91 \times 61 \times 0.2$	0.0745 (10%C)	0.000582 (0.08%C)	21.8M	125

For this study, two mesh configurations are considered in which the far-field coarse grids with a maximum grid spacing $\Delta_{max} = 0.0745$ m are refined gradually to the near-wall region. This isotropic refinement process is applied through several levels of refinement consisting of refinement boxes, and an excessive refinement offset around the airfoil body for the mesh named Fine (Table 1). The mesh properties including the observed averaged value of y^+ for these configurations are presented in Table 1. In addition, Figure 2 illustrates the boundary layer structured grid around the airfoil for the mesh named Fine (F).

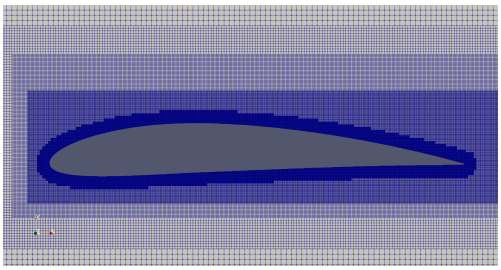

Fig. 2: The mesh resolution around the NACA 4412 airfoil.

IDDES simulations are conducted employing two distinct wall models: the APGPL wall model, which accounts for adverse pressure gradients, and an equilibrium, fully explicit wall model developed by Cai et al. [7] within the framework of LBM. In the case of the latter wall model, the boundary layer is assumed to be in an equilibrium state, and it is denoted as "WM" in this study.

The simulations using the APGPL wall model are conducted on both Medium and Fine meshes. However, the equilibrium WM wall model has only been tested on the Fine mesh. In all simulations, following an initial transient period, the averaged solution is obtained throughout 25 flow over chord time (c/U_∞) for post-processing.

The initial observation demonstrates that simulations employing the APGPL wall model possess the capability to accurately capture and highlight the phenomenon of trailing-edge separation, which is notably less pronounced in the simulations using the equilibrium WM

wall model (Figure 3). The APGPL model, by its very nature, takes into consideration the adverse pressure gradients occurring near the trailing edge, enabling a more accurate representation of the separation phenomenon in the simulated flow field. This distinction underscores the impact of employing a wall model explicitly designed to account for adverse pressure gradients.

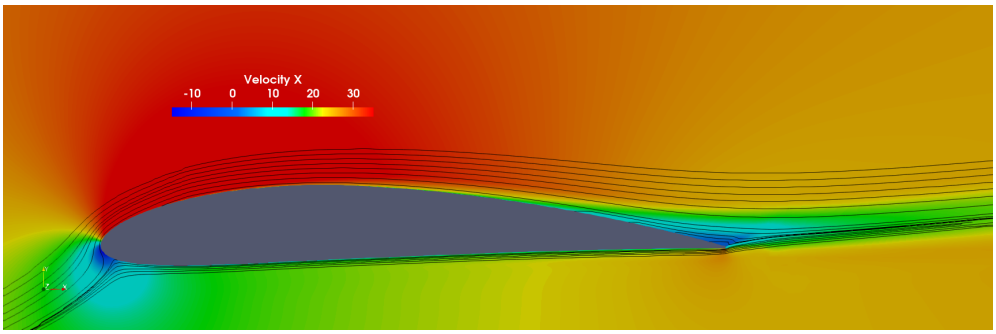

(a) IDDES - WM - F

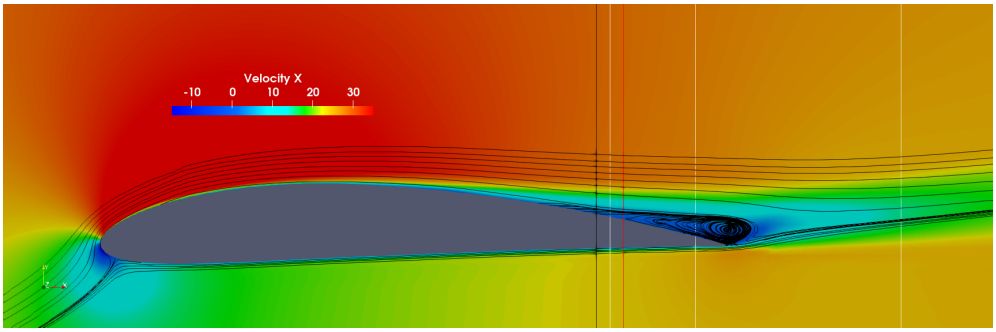

(b) IDDES - APGPL -F

Fig. 3: Streamwise velocity around the NACA-4412 airfoil for the IDDES models with an equilibrium (WM), and APGPL wall models.

Figure 4 presents a more detailed comparison between experimental data, and IDDES simulations at various positions along the airfoil: $x/c = 0.815$ (marking the onset of separation), 0.952 (within the separation region), and 1.282 in the airfoil wake. Unlike the simulation using WM, the use of the APGPL model leads to a notably more accurate prediction of the streamwise velocity and the total streamwise normal stress ($u'u'$) component within the boundary layer and in the airfoil wake. The streamwise normal stress component is calculated as the sum of the modeled and resolved contributions. In the separation region, the hybrid turbulence model behaves as WMLES, with the majority of increased turbulent motion stemming from the resolved stress component. In contrast, simulations employing the

WM model depict attached airflow over the airfoil as RANS, resulting in minimal or no contributions from resolved stress and consequently lower total stress values as compared to the experimental data.

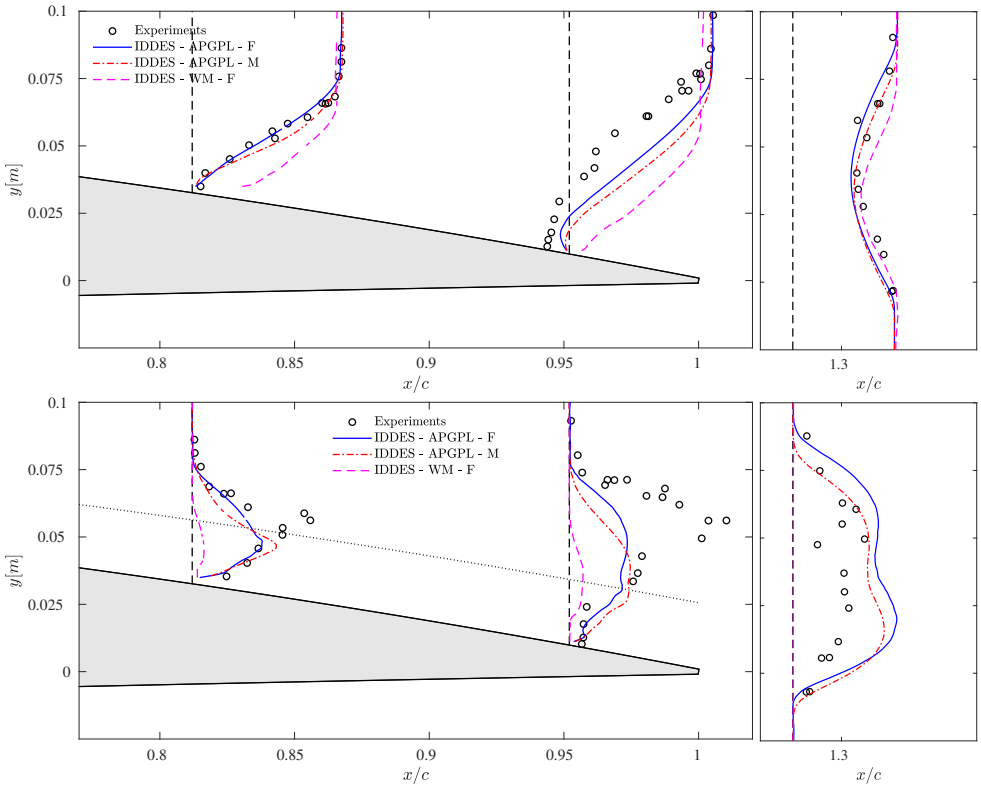

Fig. 4: Streamwise mean velocity (upper) and normal stress (lower) plot compared to experimental data for the 3D NACA 4412 airfoil case at $x/c = 0.815$, 0.952, and 1.282

The observed underprediction of the total normal stress along the airfoil in IDDES simulations utilizing the APGPL model can be attributed to mesh transitions. As illustrated in Fig 4, the thin dotted line marks the interface where the fine grids surrounding the airfoil connect with the one-level coarser grid beyond this region. This transition in mesh resolution has the potential to affect the behavior of turbulence features as they traverse this boundary. The reduced local mesh resolution in this region might lead to the dissipation of certain turbulence characteristics, resulting in the IDDES turbulence model's inability to adequately capture turbulence within the affected zone. It's worth noting that this is a significant topic of discussion, which is explored in greater detail by [41–43].

The aerodynamic coefficients and the location of separation for these simulations are compared with the reported experimental data by Wadcock [39] in Table 2. In this study, the forces acting on a body are obtained by far-field integration applied on a defined control volume encompassing the airfoil (see reference [6], for Cartesian non-body-fitted grids). The

Table 2: Lift and drag coefficient of NACA-4412 at angles of attack $\alpha = 12^{\circ}$, comparing with reference data by [44].

	C_d (err%)	C_l (err%)	X_{sep}/C (err%)	
Exp.	0.0423	1.450	0.815	
IDDES - APGPL - M	0.0458 (8.3%)	1.415 (-2.4%)	0.7928 (-2.7%)	
IDDES - APGPL - F	0.0437 (3.3%)	1.4544 (0.9%)	0.8370 (2.7%)	

application of the APGPL wall model in IDDES simulation demonstrates its ability to accurately predict the coefficient of lift and the onset of separation when compared to simulations using the WM wall model. The onset of the separation for each simulation is also illustrated by a line with the color corresponding to that simulation in Fig 3b. However, in the case of the coefficient of drag, there is a slight tendency for over-prediction, which is notably mitigated by employing a finer mesh configuration.

In this test case, the APGPL wall model significantly improves the ability to capture flow features and estimate aerodynamic forces compared to conventional wall models under equilibrium conditions. This outcome underscores the importance of accounting for adverse pressure gradients within the chosen wall model to accurately represent the distinct characteristics of the system and physical flow behaviors.

3.2 Ahmed's body

The next test case in this study is an Ahmed body model with a slant surface. This model, as a simplified car model, is a popular model to evaluate the performance of turbulence models in simulating near-wall flows in fully turbulent attached and separated boundaries. The model, as presented in Figure 5, has the size of 1044×389×288 mm in length (L), width (W), and height (H), with a slant angle of ϕ.

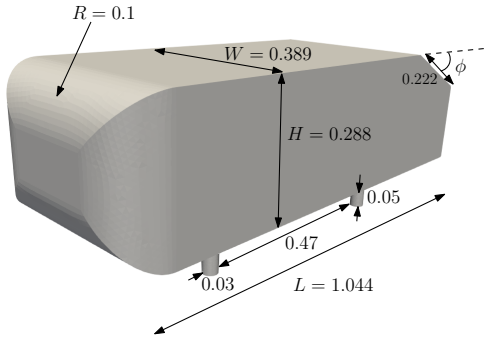

Fig. 5: The geometry of the Ahmed body (unit [m]); ϕ is the slant angle.

This study primarily focuses on the analysis of flow structures on the slanted surface and in the wake of Ahmed's body. Prior research with LBM [8] has indicated that the use of equilibrium wall models in combination with hybrid turbulence models fails to exhibit a consistent behavior and is unable to capture local flow developments. This leads to the

formation of a fully attached boundary layer on the slanted surface for the two slant angles of $\phi = 25^\circ$ and $\phi = 35^\circ$ in contrast to the reference data. Mozaffari et al. [8] observed that eliminating the wall model and applying the no-slip boundary condition yielded improved results for the test case with a slant angle of $\phi = 35^\circ$. However, for the slant angle of $\phi = 25^\circ$, this approach led to an inaccurate representation of the boundary layer and separation over the slanted surface. This observation highlights the significance of choosing an appropriate wall model and exploring the potential benefits of incorporating adverse pressure gradients into the wall model to address complex flow scenarios involving mild to significant separation and reattachment. In this section, we employ the discussed APGPL wall model (as detailed in Section 2) to account for the adverse pressure gradient. This model is used in conjunction with hybrid turbulence models within the ProLB solver to assess its effectiveness and extend its applicability to the complex separated turbulent flow around Ahmed's body.

The entire configuration is based on the ERCOFTAC benchmark test [45]. The flow's Reynolds number, determined by the body's height (H) and the incoming stream velocity of $U_\infty = 40$ m/s, corresponds to $Re_H = 7.68 \times 10^5$, aligning with the experiments conducted by Lienhart and Becker [46]. To define the inlet and outlet boundaries, a uniform stream velocity and a fixed density value are applied respectively, and symmetry boundary conditions are used in the crosswind directions. Regarding the meshing process and grid resolution, isotropic refinement with multiple levels of refinement around the body model and close to the floor is used. The final mesh consists of 45.8×10^6 cells, and this mesh is maintained for both cases with slant angles of 25° and 35°. Detailed information regarding boundary conditions, meshing details, and computational setup, can be found in [8]. IDDES simulations are conducted using the APGPL wall model around the body's surface, for the Ahmed body at slant angles of 25° and 35°. All simulations for this test case extend over 100 flow-through-time H/U_∞, and the reported solutions represent averages over the final 50 flow-through-time.

The 35° slant angle

In terms of overall fluid behavior in the wake, when employing the APGPL wall model for the IDDES simulation for the 35° slant angle, a different flow behavior emerges compared to the equilibrium wall model. Figure 6 presents the ability of the APGPL wall model to accurately capture the separation in the wake, closely resembling the result obtained by [8] when no wall model is applied, and a Dirichlet boundary condition (no-slip) is imposed. In addition, despite insufficient local mesh resolution to resolve the near-wall boundary on the slant, the topology of the flow in the wake of the IDDES simulation is in agreement with the experimental data and the reference simulation by Guilmineau et al. [47].

In addition to the two large recirculations in the wake, a small recirculation is also captured near the ending part of the slant which was also reported by Guilmineau et al. [47] in their IDDES simulation on a body-fitted grid. Regarding the length of the wake, for the present IDDES simulations, the wake is a bit larger than the reference simulation and experimental data.

To conduct a more detailed analysis of the influence of accounting for the adverse pressure gradient in the wall model, we present profiles of streamwise velocity, u_{rms}, and total turbulent kinetic energy (TKE) on the slant and in the wake of the body. These profiles are depicted in Figure 7 for the slant angle of 35°. In this analysis, these profiles are compared with the results obtained from the IDDES simulation employing an equilibrium wall model

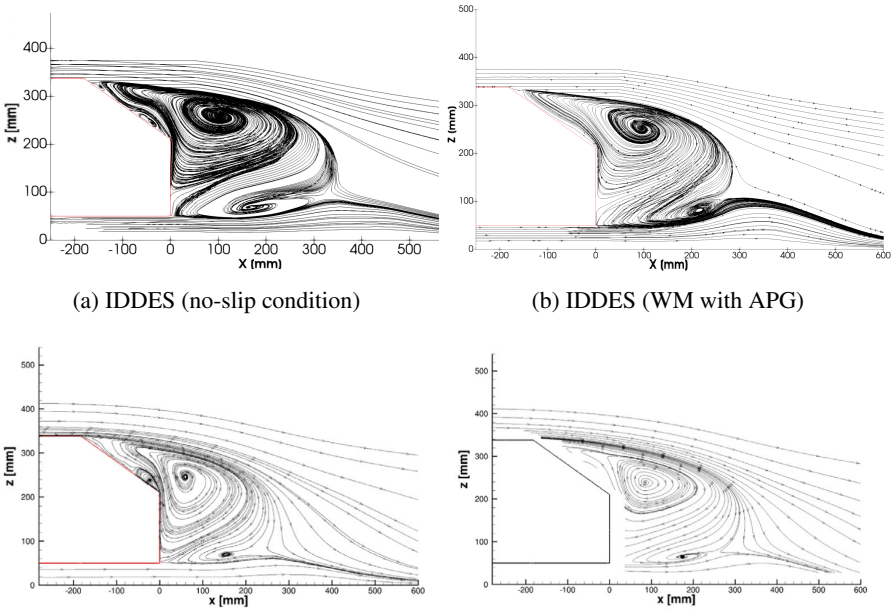

(a) IDDES (no-slip condition)

(b) IDDES (WM with APG)

(c) reference IDDES [47]

(d) Exp. [46]

Fig. 6: Streamlines in the wake of the Ahmed body with 35° slant angle. The reference figures (c, d) were copied from [47] by permission.

(referred to as WM), as well as the profiles obtained when a Dirichlet boundary condition (NS) for the wall boundary condition. It also includes data from wind tunnel experiments conducted by Lienhart and Becker [46]. The results indicate that the APGPL wall model has a significant impact on the simulation's capacity to predict flow characteristics, and it effectively addresses the challenges commonly associated with equilibrium wall models. Similar behavior is observed between APGPL and NS results in this configuration showing that the APGPL is acting as a no-slip boundary condition on the Ahmed body slant surface.

The 25° slant angle

Contrary to the 35° case, where a fully detached flow is observed on the slant surface due to the strong adverse pressure gradient between the slant and the top of the body, predicting the flow characteristics for slant angles below the critical angle ($\phi = 30°$), at which the maximum drag is obtained, presents a more complex challenge [21]. At small angles, such as 25°, a separation bubble can be identified in the initial part of the slant followed by a reattachment on the slant surface [46]. Other studies [47–49] on this geometry also confirmed the evolution of the unsteady flow structures in exchange for a change in slant angles.

Figure 8 demonstrates the ability of the combination of the APGPL wall model and hybrid RANS/LES turbulence model to accurately represent this challenging flow condition. The inclusion of the adverse pressure gradient in the wall model, which significantly influences boundary layer and separation characteristics, holds promise for improving the accurate

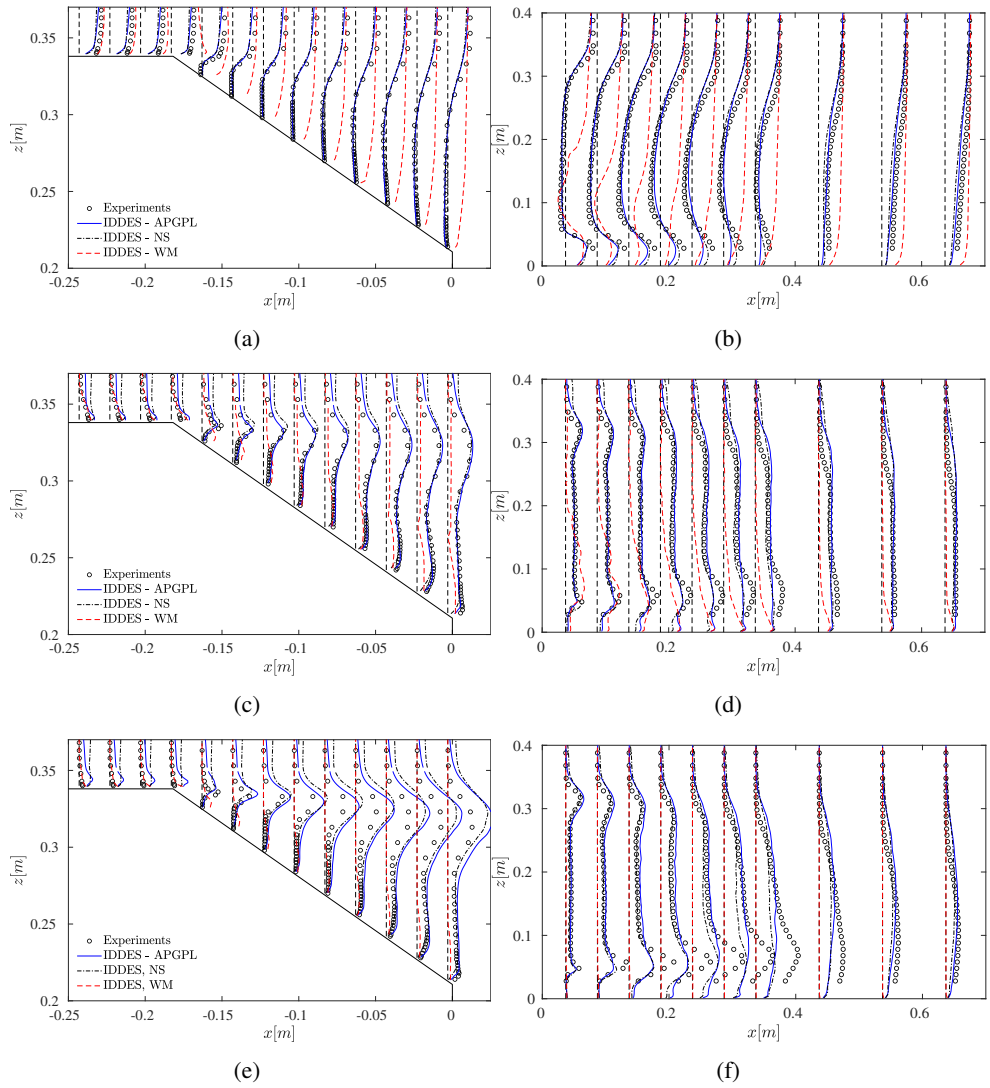

Fig. 7: Comparison of the turbulence statistics on the slant surface (left) and in the wake (right) of the Ahmed body with 35° slant angle. the mean streamwise velocity (a,b); the rms of the streamwise velocity (c,d); the total TKE (e,f).

capture of flow structures. When the no-slip boundary condition is applied, the model fails to predict reattachment on the slant, resulting in a fully detached flow. However, using the APGPL model enables recovery of the experimental behavior, featuring a minor detachment on the first half of the slant followed by reattachment on the second half. Furthermore, the flow structures in the recirculation zone and the size of this region behind Ahmed's body closely match the reference data.

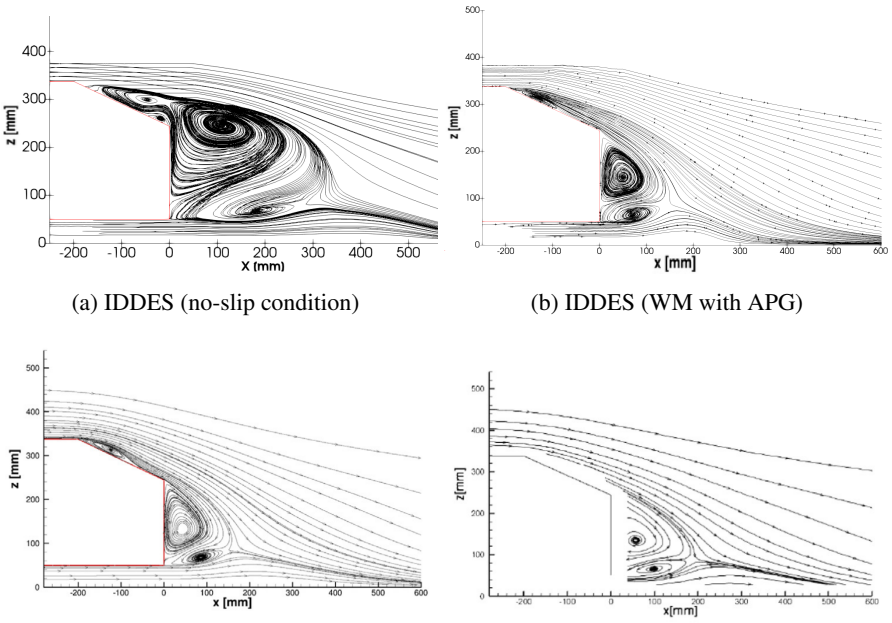

(a) IDDES (no-slip condition)

(b) IDDES (WM with APG)

(c) reference IDDES [47]

(d) Exp. [46]

Fig. 8: Streamlines in the wake of the Ahmed body with 25° slant angle. The reference figures (c, d) were copied from [47] by permission.

The analysis of the streamwise velocity, u_{rms}, and total turbulent kinetic energy (TKE) profiles on the slant and in the wake of the body provides additional evidence of the APGPL model's performance in conjunction with the hybrid RANS/LES approach (Figure 9).

Figure 10 provides a visualization of the wake by displaying isocontours of streamwise velocity in successive YZ-planes within the body's wake. In the case of a 35° slant angle, the pronounced separation along the slant is not confined to the symmetry plane. Indeed, at the end of the slant, the region with negative streamwise velocity spans the entire width of the model. This recirculation area extends far into the wake, covering more than 200 mm but less than 500 mm, consistent with reported experimental data.

However, when dealing with a 25° slant angle, due to reattachment on the slant, a region of low velocity is observed at the end of the slant. Additionally, the results reveal the presence of two counter-rotating longitudinal vortices, which originate from the edges of the slant, as in experiments. At X = 80 mm, there is a distinct region of recirculation directed back toward the body, and the IDDES simulation effectively represents and captures the trailing C-pillar vortices in the wake. The vortex structures are depicted using an isosurface of the Q-criterion in Figure 11. Moving to X = 200 mm and 500 mm, the recirculation has dissipated, and the streamwise velocity remains in good agreement with the experimental data. However, unlike the experimental results, the C-pillar vortices are no longer distinguishable. This discrepancy may be attributed to local mesh resolutions, as the mesh becomes coarser with increasing distance from the body.

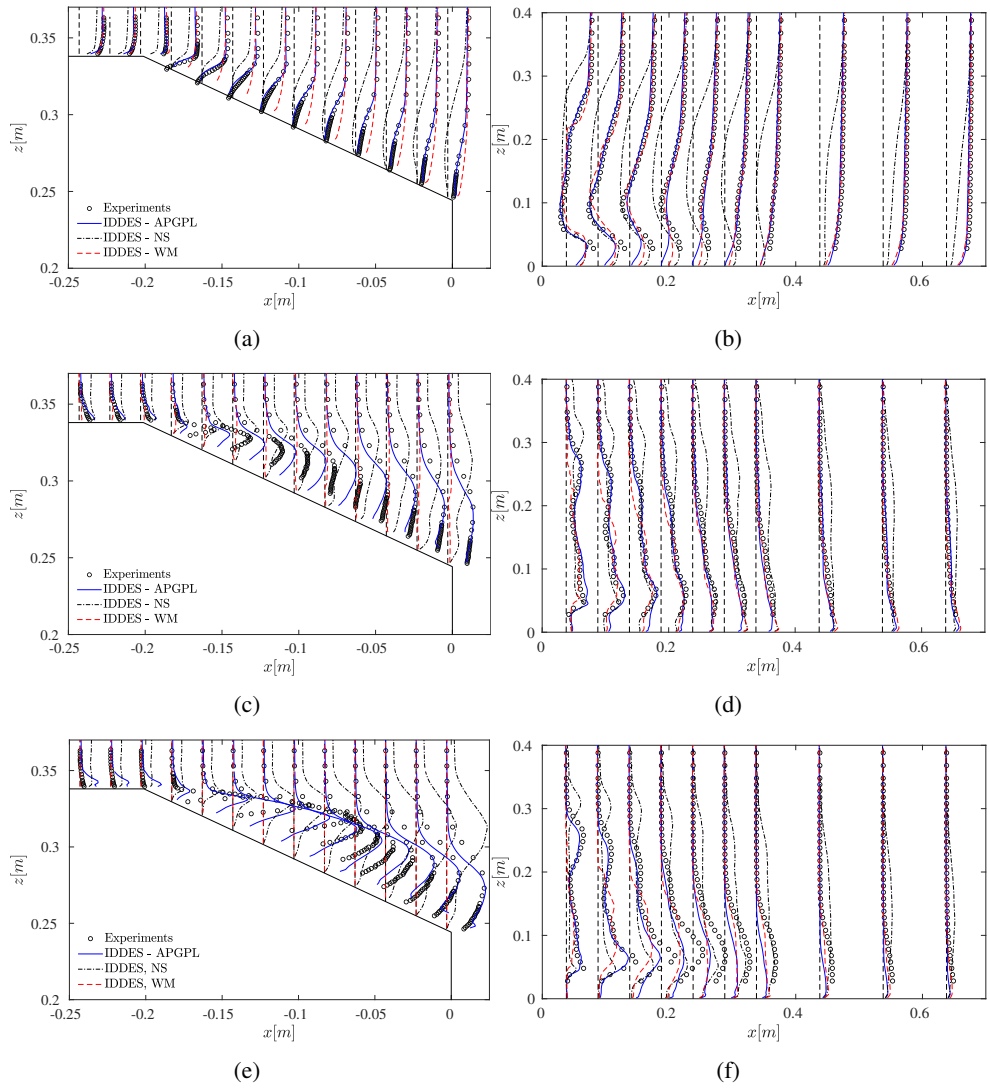

Fig. 9: Comparison of the turbulence statistics on the slant surface (left) and in the wake (right) of the Ahmed body with 25° slant angle. the mean streamwise velocity (a,b); the rms of the streamwise velocity (c,d); the total TKE (e,f).

The analyses conducted in this study have demonstrated the significant influence that the incorporation of adverse pressure gradients within the wall model exerts on the prediction of boundary layer and flow separation characteristics. Notably, these improvements were achieved without the requirement for an overly fine mesh resolution, underscoring the efficiency and affordability of the hybrid approach, combining RANS/LES turbulence models

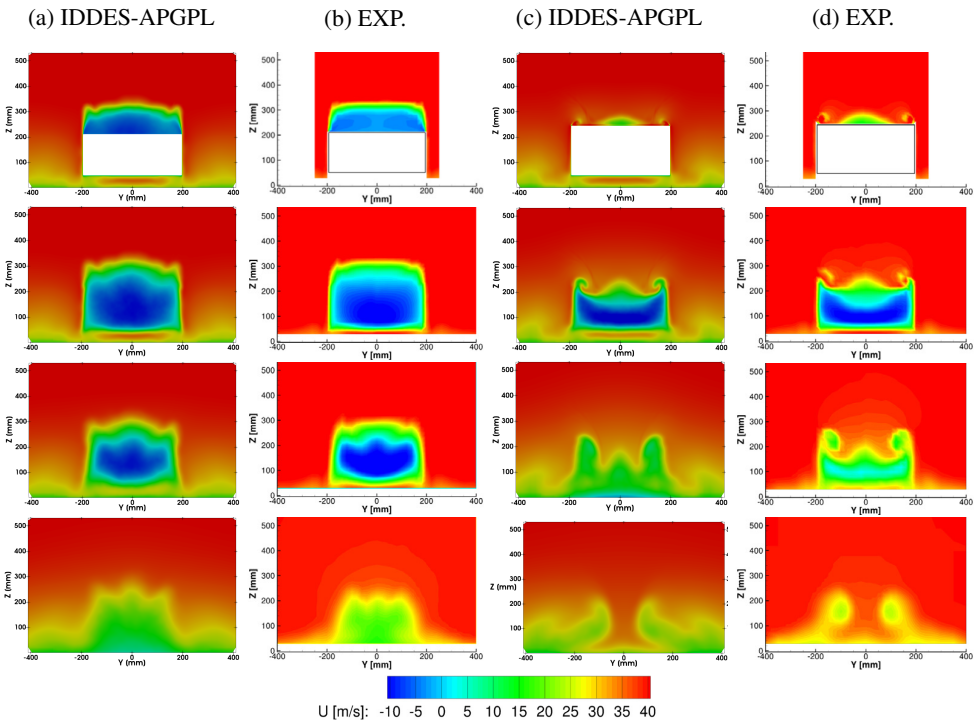

Fig. 10: Averaged streamwise velocity in successive YZ-planes in the wake of the Ahmed body. Columns represent cases with 35° slant angle (a & b), and 25° slant angle (c & d). Rows correspond to X-locations of 0 mm, 80 mm, 200 mm, and 500 mm, from top to bottom. The experiment figures were copied from [47] by permission.

with wall modeling within the Lattice Boltzmann Method (LBM). These findings emphasize the practicality of this approach for addressing complex flow phenomena.

4 Conclusion

In this study, the investigation focused on the influence of considering adverse pressure gradients within the wall model, in conjunction with the utilization of the hybrid RANS/LES turbulence model, within the framework of the Lattice Boltzmann Method, to enhance the effectiveness and reliability of simulations for turbulent separated flows. This research involved the consideration of a wall model to account for adverse pressure gradients. It was then implemented within the ProLB solver and applied in the simulation of two challenging aerodynamic external flows, to accurately capture local flow structures and detached boundary layers in these demanding scenarios. In the case of the 3D NACA-4412 airfoil near stall conditions, our findings revealed a significant improvement, in comparison to simulations that did not consider the pressure gradient effect in the wall model and relied on an equilibrium wall model instead. The results indicated a more accurate representation of the flow. Notably, the trailing edge separation was successfully captured, demonstrating the efficiency

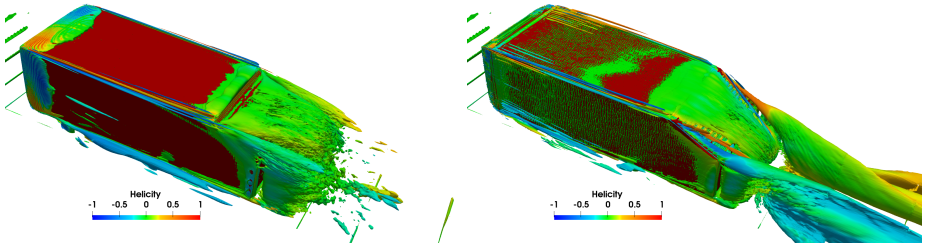

(a) $\phi = 35°$ (b) $\phi = 25°$

Fig. 11: Vortex structures around the Ahmed body visualized by iso-surface of Q-criterion ($Q = 5000$).

of this approach. Furthermore, the performance of this methodology was assessed for turbulent flows over the Ahmed body, with two slant angles. The simulations closely aligned with the reported data of wind tunnel experiments, particularly for a slant angle of 35°, characterized by massive flow separation on the slant surface. Additionally, at a more complex slant angle of 25°, the simulations correctly depicted a small separation at the initial portion of the slanted surface, followed by reattachment. A comprehensive analysis of the flow on the slanted surface and within the wake of the Ahmed body reaffirmed the promise of incorporating pressure gradient effects within the formulation of wall models. Given the promising outcomes and insights derived from this study, the logical next step involves the expansion of the application of these wall models to internal turbulent flows. This extension has the potential to yield valuable insights and improvements in a broader range of fluid flow scenarios, further enhancing the applicability and robustness of LBM simulations in the field of computational fluid dynamics.

Acknowledgment

This research was supported by the French project BALBUZARD funded by DGAC and supported by Next Generation EU in the frame of "Plan national de Relance et de Résilience français (PNRR)". This project was provided with computer and storage resources by GENCI at TGCC thanks to the grant 2023-A0152A07679 on the supercomputer Joliot Curie SKL/ROME partition. Centre de Calcul Intensif d'Aix-Marseille is acknowledged for granting access to its high-performance computing resources.

Funding

N/A

Conflict of Interest

N/A

Ethical approval

N/A

Informed consent

N/A

Author contribution

Not applicable / Appreciating the collaborative effort that has led to the completion of this manuscript, the authors refrain from providing a detailed breakdown of individual contributions in this statement.

Data Availability Statement

Not applicable / The data associated with this manuscript is not publicly available. However, it can be made accessible upon request from the authors.

References

[1] Deardorff, J.W.: A numerical study of three-dimensional turbulent channel flow at large Reynolds numbers. Journal of Fluid Mechanics **41**(2), 453–480 (1970) https://doi.org/10.1017/S0022112070000691

[2] Schumann, U.: Subgrid scale model for finite difference simulations of turbulent flows in plane channels and annuli. Journal of computational physics **18**(4), 376–404 (1975) https://doi.org/10.1016/0021-9991(75)90093-5

[3] Spalding, D.B.: A single formula for the law of the wall. Journal of Applied Mechanics **28**(3), 455–458 (1961) https://doi.org/10.1115/1.3641728

[4] Werner, H., Wengle, H.: Large-eddy simulation of turbulent flow over and around a cube in a plate channel. In: Turbulent Shear Flows 8: Selected Papers from the Eighth International Symposium on Turbulent Shear Flows, Munich, Germany, September 9–11, 1991, pp. 155–168 (1993). https://doi.org/10.1007/978-3-642-77674-8_12 . Springer

[5] Seena, A., Afzal, N.: Power law velocity and temperature profiles in a fully developed turbulent channel flow. Journal of heat transfer **130**(9), 091701 (2008)

[6] Wilhelm, S., Jacob, J., Sagaut, P.: An explicit power-law-based wall model for lattice Boltzmann method–Reynolds-averaged numerical simulations of the flow around airfoils. Physics of Fluids **30**(6), 065111 (2018) https://doi.org/10.1063/1.5031764

[7] Cai, S.-G., Sagaut, P.: Explicit wall models for large eddy simulation. Physics of Fluids **33**(4), 041703 (2021) https://doi.org/10.1007/s10494-020-00181-7

[8] Mozaffari, S., Cai, S.-G., Jacob, J., Sagaut, P.: Lattice Boltzmann k-ω SST based hybrid RANS/LES simulations of turbulent flows (submitted). Journal of Computational Physics **205**(1), 131–156 (2023)

[9] Afzal, N., Gersten, K.: Wake layer in a turbulent boundary layer with pressure gradient: a new approach. Fluid Mechanics and Its Applications **37**, 95–118 (1996)

[10] Skote, M., Henningson, D.S.: Direct numerical simulation of a separated turbulent boundary layer. Journal of Fluid Mechanics **471**, 107–136 (2002) https://doi.org/10.1017/S0022112002002173

[11] Gungor, A.G., Maciel, Y., Simens, M., Soria, J.: Scaling and statistics of large-defect adverse pressure gradient turbulent boundary layers. International Journal of Heat and Fluid Flow **59**, 109–124 (2016) https://doi.org/10.1016/j.ijheatfluidflow.2016.03.004

[12] Stratford, B.: The prediction of separation of the turbulent boundary layer. Journal of fluid mechanics **5**(1), 1–16 (1959) https://doi.org/10.1017/S0022112059000015

[13] Simpson, R.L., Chew, Y.-T., Shivaprasad, B.: The structure of a separating turbulent boundary layer. Part 1. Mean flow and Reynolds stresses. Journal of Fluid Mechanics **113**, 23–51 (1981) https://doi.org/10.1017/S002211208100339X

[14] Skote, M., Henningson, D.S., Henkes, R.A.: Direct numerical simulation of self-similar turbulent boundary layers in adverse pressure gradients. Flow, turbulence and combustion **60**(1), 47–85 (1998) https://doi.org/10.1023/A:1009934906108

[15] Schlichting, H., Gersten, K.: Boundary-Layer Theory, 8th edn. Springer, Berlin, Heidelberg (2016). https://doi.org/10.1007/978-3-662-52919-5

[16] Wang, M., Moin, P.: Dynamic wall modeling for large-eddy simulation of complex turbulent flows. Physics of Fluids **14**(7), 2043–2051 (2002) https://doi.org/10.1063/1.1476668

[17] Hou, Y., Angland, D.: A comparison of wall functions for bluff body aeroacoustic simulations. In: 22nd AIAA/CEAS Aeroacoustics Conference, p. 2771 (2016). https://doi.org/10.2514/6.2016-2771

[18] Marsden, O., Bogey, C., Bailly, C.: Direct noise computation of the turbulent flow around a zero-incidence airfoil. AIAA journal **46**(4), 874–883 (2008) https://doi.org/10.2514/1.29825

[19] Zhang, C., Sanjose, M., Moreau, S.: Improvement of the near wall treatment in large eddy simulation for aeroacoustic applications. In: 2018 AIAA/CEAS Aeroacoustics Conference, p. 3795 (2018). https://doi.org/10.2514/6.2018-3795

[20] Wilhelm, S., Jacob, J., Sagaut, P.: A new explicit algebraic wall model for LES of turbulent flows under adverse pressure gradient. Flow, Turbulence and Combustion **106**(1),

1–35 (2021) https://doi.org/10.1007/s10494-020-00181-7

[21] Menter, F.R., Hüppe, A., Flad, D., Garbaruk, A.V., Matyushenko, A.A., Stabnikov, A.S.: Large Eddy Simulations for the Ahmed Car at 25° Slant Angle at Different Reynolds Numbers. Flow, Turbulence and Combustion (2023) https://doi.org/10.1007/s10494-023-00472-9

[22] CS: ProLB website. http://www.prolb-cfd.com (2017)

[23] Dong, Z.-Q., Wang, L.-P., Peng, C., Chen, T.: A systematic study of hidden errors in the bounce-back scheme and their various effects in the lattice Boltzmann simulation of viscous flows. Physics of Fluids **34**(9), 093608 (2022) https://doi.org/10.1063/5.0106954

[24] Jacob, J., Malaspinas, O., Sagaut, P.: A new hybrid recursive regularised Bhatnagar–Gross–Krook collision model for lattice Boltzmann method-based large eddy simulation. Journal of Turbulence **19**(11-12), 1051–1076 (2018) https://doi.org/10.1080/14685248.2018.1540879

[25] Krüger, T., Kusumaatmaja, H., Kuzmin, A., Shardt, O., Silva, G., Viggen, E.M.: The lattice Boltzmann method. Springer International Publishing **10**(978-3), 4–15 (2017) https://doi.org/10.1007/978-3-319-44649-3

[26] Cai, S.-G., Degrigny, J., Boussuge, J.-F., Sagaut, P.: Coupling of turbulence wall models and immersed boundaries on Cartesian grids. Journal of Computational Physics **429**, 109995 (2021) https://doi.org/10.1016/j.jcp.2020.109995

[27] Degrigny, J., Cai, S.-G., Boussuge, J.-F., Sagaut, P.: Improved wall model treatment for aerodynamic flows in LBM. Computers & Fluids **227**, 105041 (2021) https://doi.org/10.1016/j.compfluid.2021.105041

[28] Chaouat, B.: The state of the art of hybrid RANS/LES modeling for the simulation of turbulent flows. Flow, turbulence and combustion **99**, 279–327 (2017)

[29] Spalart, P.R.: Comments on the feasibility of LES for wings, and on a hybrid RANS/LES approach. In: Proceedings of First AFOSR International Conference on DNS/LES (1997). Greyden Press

[30] Spalart, P.R., Allmaras, S.: A one-equation turbulence model for aerodynamic flows. In: 30^{th} Aerospace Sciences Meeting and Exhibit, p. 439 (1992). https://doi.org/10.2514/6.1992-439

[31] Squires, K.D., Forsythe, J.R., Spalart, P.R.: Detached-eddy simulation of the separated flow around a forebody cross-section. In: Direct and Large-Eddy Simulation IV, pp. 481–500. Springer, Dordrecht (2001). https://doi.org/10.1007/978-94-017-1263-7_57

[32] Menter, F.R., Kuntz, M.: Adaptation of eddy-viscosity turbulence models to unsteady

separated flow behind vehicles. In: The Aerodynamics of Heavy Vehicles: Trucks, Buses, and Trains, pp. 339–352. Springer, Berlin, Heidelberg (2004). https://doi.org/10.1007/978-3-540-44419-0_30

[33] Gritskevich, M.S., Garbaruk, A.V., Schütze, J., Menter, F.R.: Development of DDES and IDDES formulations for the k-ω shear stress transport model. Flow, turbulence and combustion **88**(3), 431–449 (2012) https://doi.org/10.1007/s10494-011-9378-4

[34] Shur, M.L., Spalart, P.R., Strelets, M.K., Travin, A.K.: A hybrid RANS-LES approach with delayed-DES and wall-modelled LES capabilities. International Journal of Heat and Fluid Flow **29**(6), 1638–1649 (2008) https://doi.org/10.1016/j.ijheatfluidflow.2008.07.001

[35] Spalart, P.R., Deck, S., Shur, M.L., Squires, K.D., Strelets, M.K., Travin, A.K.: A new version of detached-eddy simulation, resistant to ambiguous grid densities. Theoretical and Computational Fluid Dynamics **20**(3), 181–195 (2006) https://doi.org/10.1007/s00162-006-0015-0

[36] Menter, F.R.: Two-equation eddy-viscosity turbulence models for engineering applications. AIAA journal **32**(8), 1598–1605 (1994) https://doi.org/10.2514/3.12149

[37] Cai, S.-G., Mozaffari, S., Jacob, J., Sagaut, P.: Application of immersed boundary based turbulence wall modeling to the Ahmed body aerodynamics. Physics of Fluids **34**(9), 095106 (2022) https://doi.org/10.1063/5.0098232

[38] Yang, X.I.A., Sadique, J., Mittal, R., Meneveau, C.: Integral wall model for large eddy simulations of wall-bounded turbulent flows. Physics of Fluids **27**(2), 025112 (2015) https://doi.org/10.1063/1.4908072

[39] Wadcock, A.J.: Investigation of low-speed turbulent separated flow around airfoils. Technical report, NASA-CR-177450. Ames Research Center, NASA (1987)

[40] Xu, H., Sagaut, P.: Analysis of the absorbing layers for the weakly-compressible lattice Boltzmann methods. Journal of Computational Physics **245**, 14–42 (2013) https://doi.org/10.1016/j.jcp.2013.02.051

[41] Piomelli, U., Kang, S., Ham, F., Iaccarino, G.: Effect of discontinuous filter width in large-eddy simulations of plane channel flow. Studying turbulence using numerical databases XI, 151–162 (2006)

[42] Goodfriend, E., Chow, F., Vanella, M., Balaras, E.: Large-eddy simulation of decaying isotropic turbulence across a grid refinement interface using explicit filtering and reconstruction. Journal of Turbulence **14**(12), 58–76 (2013) https://doi.org/10.1080/14685248.2013.867964

[43] Mozaffari, S., Guilmineau, E., Visonneau, M., Wackers, J.: Average-based mesh adaptation for hybrid RANS/LES simulation of complex flows. Computers & Fluids **232**,

105202 (2022) https://doi.org/10.1016/j.compfluid.2021.105202

[44] Shur, M., Spalart, P., Strelets, M., Travin, A.: Detached-eddy simulation of an airfoil at high angle of attack. In: Engineering Turbulence Modelling and Experiments 4, pp. 669–678. Elsevier, Oxford (1999). https://doi.org/10.1016/B978-008043328-8/50064-3

[45] ERCOFTAC: Ahmed Body. https://www.kbwiki.ercoftac.org/w/index.php/Description_AC1-05

[46] Lienhart, H., Becker, S.: Flow and turbulence structure in the wake of a simplified car model. SAE transactions, 785–796 (2003)

[47] Guilmineau, E., Deng, G., Leroyer, A., Queutey, P., Visonneau, M., Wackers, J.: Assessment of hybrid RANS-LES formulations for flow simulation around the Ahmed body. Computers & Fluids **176**, 302–319 (2018) https://doi.org/10.1016/j.compfluid.2017.01.005

[48] Liu, K., Zhang, B., Zhang, Y., Zhou, Y.: Flow structure around a low-drag Ahmed body. Journal of Fluid Mechanics **913** (2021) https://doi.org/10.1017/jfm.2020.1136

[49] Zhang, B., Zhou, Y., To, S.: Unsteady flow structures around a high-drag Ahmed body. Journal of Fluid Mechanics **777**, 291–326 (2015) https://doi.org/10.1017/jfm.2015.332